A hybrid plasmonic waveguide for subwavelength confinement and long-range propagation

R. F. OULTON, V. J. SORGER, D. A. GENOV, D. F. P. PILE AND X. ZHANG*

NSF Nanoscale Science and Engineering Center, 3112 Etcheverry Hall, University of California, Berkeley, California 94720, USA
*e-mail: xiang@berkeley.edu

Published online: 11 July 2008; doi:10.1038/nphoton.2008.131

The emerging field of nanophotonics[1] addresses the critical challenge of manipulating light on scales much smaller than the wavelength. However, very few feasible practical approaches exist at present. Surface plasmon polaritons[2,3] are among the most promising candidates for subwavelength optical confinement[3–10]. However, studies of long-range surface plasmon polaritons have only demonstrated optical confinement comparable to that of conventional dielectric waveguides, because of practical issues including optical losses and stringent fabrication demands[3,11–13]. Here, we propose a new approach that integrates dielectric waveguiding with plasmonics. The hybrid optical waveguide consists of a dielectric nanowire separated from a metal surface by a nanoscale dielectric gap. The coupling between the plasmonic and waveguide modes across the gap enables 'capacitor-like' energy storage that allows effective subwavelength transmission in non-metallic regions. In this way, surface plasmon polaritons can travel over large distances (40–150 μm) with strong mode confinement (ranging from $\lambda^2/400$ to $\lambda^2/40$). This approach is fully compatible with semiconductor fabrication techniques and could lead to truly nanoscale semiconductor-based plasmonics and photonics.

The need for fast, compact and efficient light sources and detectors with high spatial and temporal resolution has motivated research into optical structures capable of guiding light with deep subwavelength confinement. Photonic crystals[14–16] have been used to guide light, although fundamentally, the confinement is limited to the order of a wavelength in each direction. Subwavelength confinement along one dimension has been shown in all-dielectric coupled silicon waveguides[17]. This geometry is of fundamental importance in nanophotonics, although the relatively large portion of energy propagating in the surrounding regions may restrict the compactness of the waveguide. On the other hand, plasmonic waveguides can provide subwavelength confinement by storing optical energy in electron oscillations within dissipative metallic regions[2–13,18]. This, however, leads to high optical loss, which is further exacerbated when high-permittivity dielectric materials such as semiconductors are involved[18]. Consequently, semiconductor-based plasmonics faces a fundamental challenge at telecommunications and visible frequencies.

In this letter, we report a hybrid plasmonic waveguide capable of subwavelength confinement in two dimensions with low propagation loss. The hybrid mode can be strongly confined to sizes more than 100 times smaller than the area of a diffraction-limited spot, while maintaining propagation distances exceeding those of surface plasmon polaritons (SPPs) of the equivalent high-permittivity dielectric–metal interface, which are only confined in one dimension. Moreover, by tuning the geometrical properties of this structure, we can increase the propagation distance up to the millimetre range while still maintaining moderate confinement. This approach naturally extends the capabilities of both plasmonics and semiconductor photonics and can be applied to subwavelength laser devices, such as visible nanolasers[19,20] and terahertz lasers[21] as well as optically integrated circuits[22].

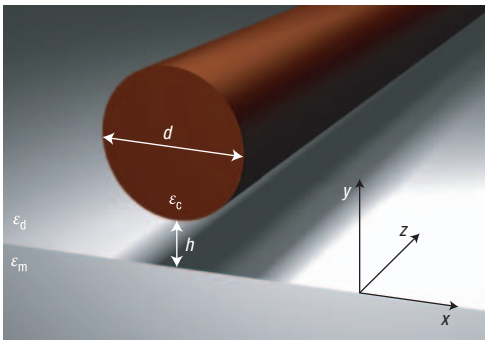

Figure 1 The hybrid optical waveguide. A dielectric cylindrical nanowire[23] of permittivity ε_c and diameter d is separated from a metallic half-space of permittivity ε_m by a nanoscale dielectric gap of permittivity ε_d and width h. The upper medium is a dielectric of permittivity ε_d. $\varepsilon_c = 12.25$ (GaAs) and $\varepsilon_d = 2.25$ (SiO_2) at the telecommunications wavelength $\lambda = 1{,}550$ nm. The metallic region is silver with a permittivity of $-129 + 3.3i$ (ref. 24). The centre of the cylinder defines the origin ($x = y = 0$).

The hybrid waveguide geometry shown in Fig. 1 consists of a high-permittivity semiconductor nanowire[23] (cylinder waveguide) embedded in a low-permittivity dielectric near a metal surface (SPP waveguide)[25]. In the following study, we vary the cylinder diameter, d, and the dielectric gap width, h, between the cylinder and the metal plane to control the propagation distance, L_m,

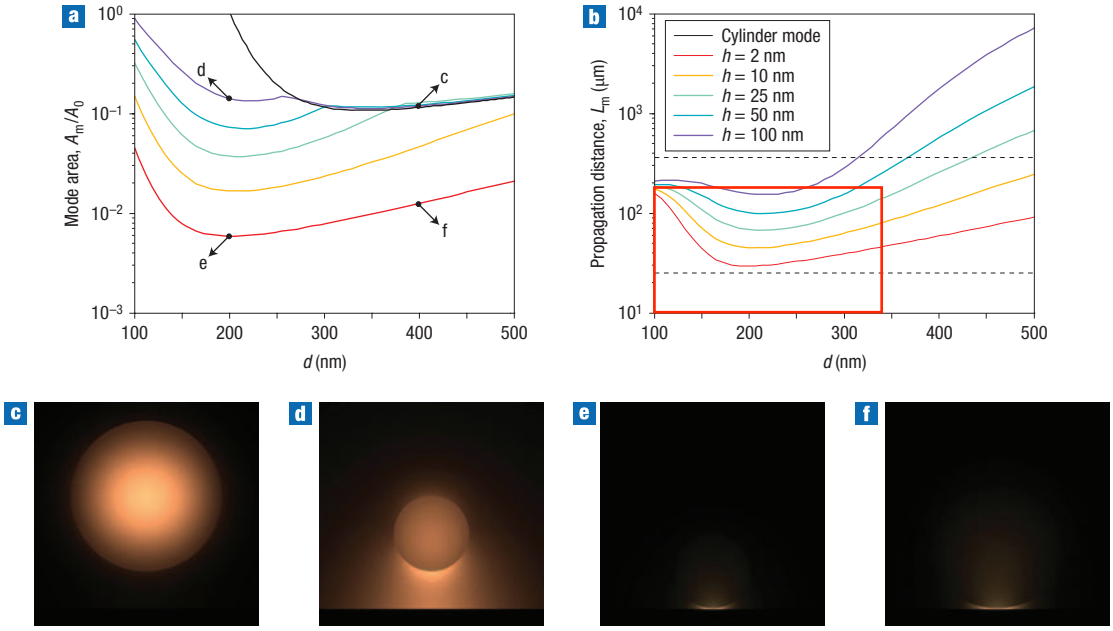

Figure 2 Propagation distance, mode area and field distributions of the hybrid mode. a, Mode area, A_m/A_0 (see equation (5)) versus cylinder diameter d for different gap width h (coloured lines), compared with the mode area of a pure cylinder mode (black line). **b**, The hybrid mode's propagation distance (coloured lines), compared with those of pure SPP modes at metal–oxide (upper dashed black line) and metal–semiconductor (lower dashed black line) interfaces. **c**–**f**, Electromagnetic energy density distributions for $[d,h] = [400, 100]$ nm (**c**), $[d,h] = [200, 100]$ nm (**d**), $[d,h] = [200, 2]$ nm (**e**) and $[d,h] = [400, 2]$ nm (**f**), corresponding to the points indicated in panel **a**. The key in the inset of **b** applies throughout this letter.

mode area, A_m, and electromagnetic field distribution of a single hybrid mode at the telecommunications wavelength, $\lambda = 1{,}550$ nm. Figure 2a,b shows the dependence of propagation distance and normalized mode area, respectively, on d and h using the finite element method (see Methods). For a large cylinder diameter and gap width ($d > 200$ nm, $h > 50$ nm), the hybrid waveguide supports a low-loss cylinder-like mode with electromagnetic energy confined to the high-permittivity dielectric core (Fig. 2c). Conversely, a small-diameter cylinder ($d < 200$ nm) results in an SPP-like mode with very weak localization parallel to the metal surface and suffering loss comparable to that of uncoupled SPPs. At moderate cylinder diameters ($d \simeq 200$ nm), mode coupling results in a new hybrid mode that features both cylinder and SPP characteristics; namely, its electromagnetic energy is distributed over both the cylinder and the adjacent metal–dielectric interface (Fig. 2d). However, when reducing the gap towards the nanometre scale, the hybrid mode no longer displays characteristics of either the cylinder or the SPP mode; instead, it is strongly confined in two dimensions within the gap (Fig. 2e,f). What is interesting here is that, despite this strong confinement, the hybrid mode's propagation length exceeds that of SPPs of the equivalent metal–semiconductor interface (Fig. 2b).

Evidently, the gap provides the means to store electromagnetic energy, leading to subwavelength optical guiding with low mode loss. (See animation in Supplementary Information.) This is further confirmed by resolving the electromagnetic energy density in more detail (Fig. 3). The proportion of the mode's energy residing within the gap is 15% for $h = 2$ nm (Fig. 2e), up to 20% for $h = 100$ nm (Fig. 2d), where we define the gap region as the area of low-permittivity dielectric directly beneath the cylinder and above the metal. The strong energy confinement in the gap region occurs for two reasons. First, it arises from the continuity of the displacement field at the material interfaces, which leads to a strong normal electric-field component in the gap[17]. Second, in both uncoupled SPP and cylinder geometries, the electric-field components normal to the material interfaces are dominant, amplifying the first effect. In fact, the dielectric discontinuity at the semiconductor–oxide interface produces a polarization charge[26] that interacts with the plasma oscillations of the metal–oxide interface; that is, the gap region has an effective optical capacitance, similar to that of a closely spaced metallic wire and plane.

In order to gain a deeper understanding, we analysed the dependence of the hybrid mode's effective index, $n_{hyb}(d,h)$, on d and h. Figure 4a depicts the variation of the effective index for the same set of parameters as in Fig. 2. Naturally, in the limits of cylinder-like and SPP-like modes, the effective index approaches that of a pure cylinder, $n_{cyl}(d)$, or an SPP, n_{spp}, mode (Fig. 4a). At the same time, the hybrid mode's effective index is always larger than that of the underlying cylinder and SPP waveguide modes, indicating a behaviour typical of a coupled mode system with mode 'splitting' into symmetric and antisymmetric hybrid modes[27,28] with effective indices $n_{\pm}(d,h)$ (see Methods). Interestingly, the lower ('antisymmetric') branch of the system is 'cut off' as the lower index hybrid mode cannot exist for effective indices $n_{-}(d,h) < n_{spp}$. The high index ('symmetric') mode is the only bound solution in this geometry for a single-mode cylinder waveguide. (Note that hybridization lifts the degeneracy of the cylinder's fundamental mode, and the second mode is cut off when the coupling is strong).

Using a coupled-mode theory, we can describe the hybrid mode, to a first approximation, as a 'superposition' of the cylinder waveguide (without the metallic region) and the SPP waveguide (with no cylinder) modes,

$$\psi_{\pm}(d,h) = a_{\pm}(d,h)\psi_{cyl}(d) + b_{\pm}(d,h)\psi_{spp} \qquad (1)$$

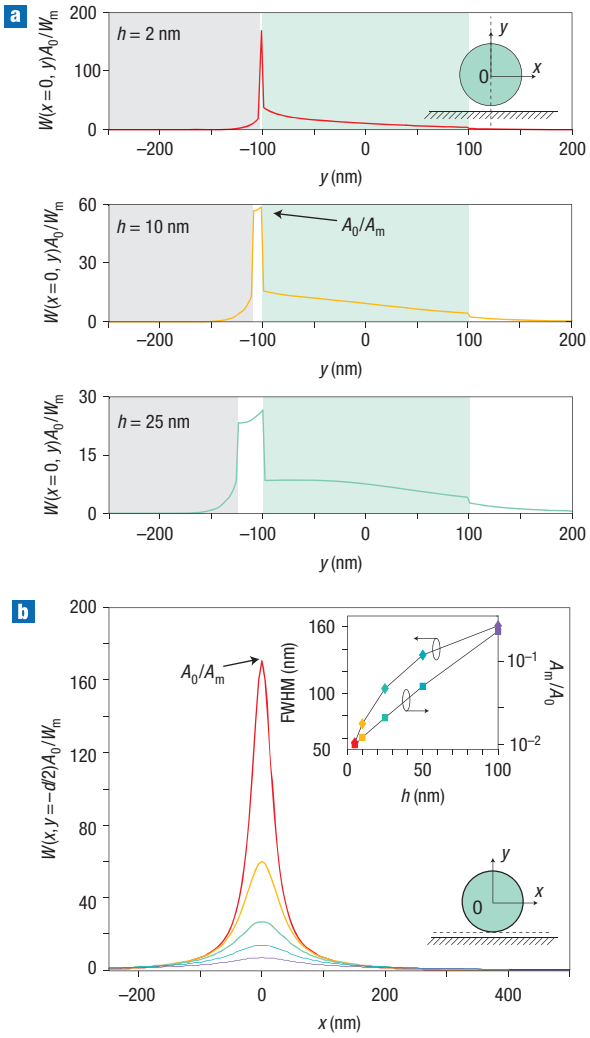

Figure 3 Confinement in the dielectric gap region in the *x* and *y* directions. **a**, Normalized energy density along $x = 0$ (dashed line in inset) shows the confinement in the low-index dielectric region (no shading). The shaded grey and green areas represent the metal and semiconductor regions, respectively. **b**, The energy density along $y = -d/2$ (dashed line in lower right inset) also shows subwavelength localization. The upper right inset shows the full-width at half-maximum (FWHM) of the mode along $y = -d/2$ and the normalized mode area, A_m/A_0, as a function of h.

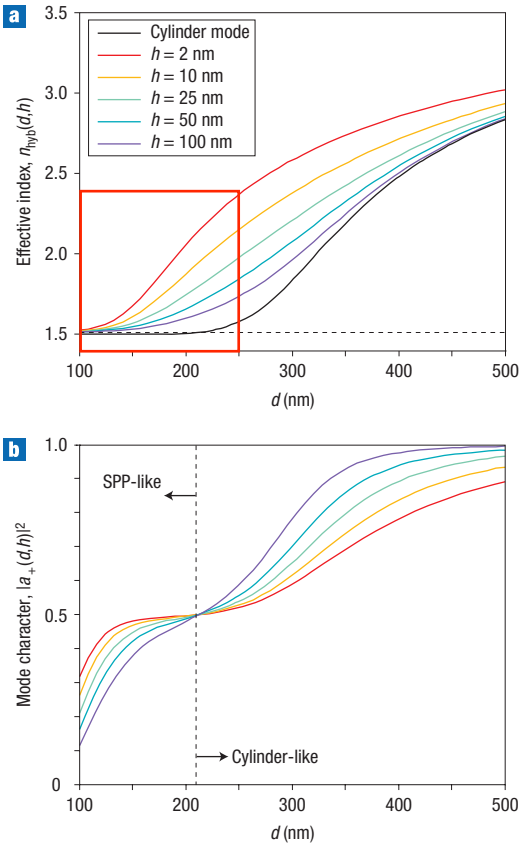

Figure 4 The hybridization of the dielectric cylinder and SPP modes as modelled by coupled mode theory. **a**, The effective index of the hybrid waveguide for a range of gap widths h and cylinder diameters d (coloured lines) compared with the analytical effective indices of the pure cylinder, $n_{cyl}(d)$ (ref. 29; black solid line), and pure SPP, n_{spp} (black broken line), modes (see Methods). **b**, The cylinder mode character determined from equation (2). When $|a_+(d,h)|^2 > 0.5$ the mode is cylinder-like and when $|a_+(d,h)|^2 < 0.5$, the mode is SPP-like. Maximum coupling occurs near $d = 200$ nm, where the hybrid mode consists of equal proportions of cylinder and SPP modes; that is, $|a_+(d,h)|^2 = 0.5$.

where $a_\pm(d,h)$ and $b_\pm(d,h) = \sqrt{1 - |a_\pm(d,h)|^2}$ are the amplitudes of the constituent cylinder, $\psi_{cyl}(d)$, and SPP, ψ_{spp}, modes respectively (see Methods). The square norm of the cylinder mode amplitude $|a_+(d,h)|^2$ is a measure of the 'character' of the hybrid mode, that is, the degree to which the guided mode is cylinder-like (or SPP-like):

$$|a_+(d,h)|^2 = \frac{n_{hyb}(d,h) - n_{spp}}{(n_{hyb}(d,h) - n_{cyl}(d)) + (n_{hyb}(d,h) - n_{spp})} \quad (2)$$

In this respect, the mode is cylinder-like for $|a_+(d,h)|^2 > 0.5$ and SPP-like otherwise (Fig. 3b). Although the mode character predicts the transition between cylinder-like and SPP-like modes, it also correlates the point of strongest coupling, near $d = 200$ nm, with the minimum of both mode area and propagation distance (Fig. 4). At the critical coupling diameter d_c, the hybrid mode has equal SPP and cylinder characteristics ($|a_+(d,h)|^2 = 0.5$), corresponding to the condition $n_{cyl}(d) = n_{spp}$, indicating that polarization charge and plasma oscillations move in phase and maximize the effective optical capacitance of the waveguide. For $d \simeq d_c$, mode areas more than two orders of magnitude ($6 \times 10^{-3} A_0$) smaller than the diffraction-limited area in free space, $A_0 = \lambda^2/4$, are achievable (Fig. 2a). As the gap width decreases further, $h \mapsto 0$, we can expect the reduction in mode area to continue with the propagation distance, tending to that of a semiconductor–metal interface, subject to constraints of non-local effects.

Figure 5 shows a parametric plot of normalized mode area A_m/A_0 versus normalized propagation distance L_m/λ, for a variety of plasmonic waveguides. Note that this plot is independent of a waveguide's structural parameters, allowing a fair comparison of waveguide geometries. Furthermore, by retaining the absolute values of L_m and A_m, this representation provides a more powerful comparative tool than a single-valued figure of merit[30] such as $\sim L_m/\sqrt{A_m}$.

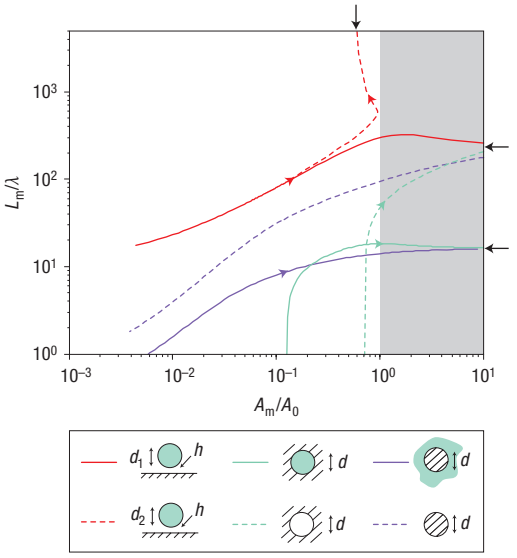

Figure 5 A plot of normalized mode area versus normalized propagation distance enables a comparison of various plasmonic waveguides. Here we compare the hybrid mode (red lines) with dielectric-clad silver nanowires[4–6] (blue lines) and silver-clad dielectric nanowires[5,6] (green lines). The permittivities of the nanowire waveguides are ε_d (dashed lines) and ε_c (solid lines). A trajectory shows a range of one structural parameter: $h = [1,1 \times 10^4]$ nm, $d_1 = 200$ nm and $d_2 = 215$ nm for the hybrid mode (d_1 and d_2 correspond to two possible asymptotic solutions as $h \mapsto \infty$); $d = [10,1 \times 10^4]$ nm for the NW waveguides. Arrows indicate increasing waveguide parameter. Black arrows on the right show asymptotic values for the propagation distances of SPPs at oxide–silver and semiconductor–silver interfaces. The black arrow on top is the mode area for the d_2 hybrid mode for $h \mapsto \infty$.

Each trajectory in Fig. 5 represents a plasmonic waveguide over the range of a structural parameter; here, we compare the hybrid waveguide with dielectric clad metal nanowires[4–6] and metal clad dielectric nanowires[5,6]. Waveguides with the best performance have trajectories towards the top left of the plot. Clearly, the hybrid waveguide outperforms the other geometries considered by at least an order of magnitude in propagation length for comparable mode areas. We have also compared the hybrid waveguide with other plasmonic waveguides, including wedge and groove structures (see Supplementary Information). In these cases, the hybrid waveguide also shows longer propagation distances for similar degrees of confinement.

In conclusion, we have proposed a new approach for low-loss deep-subwavelength light transport. By controlling the hybridization of the fundamental mode of a dielectric cylinder with the SPP of a dielectric–metal interface, we can simultaneously achieve subwavelength confinement and long-range propagation. We have further shown that the new hybrid waveguide is superior to other plasmonic waveguides in the literature. Our hybrid approach enables the integration of high-gain semiconductor materials and plasmonics and could therefore lead to the implementation of waveguide loss compensation techniques[8,18] as well as other schemes for actively manipulating truly nanoscale optical fields. The potential for single-mode operation in conjunction with deep-subwavelength mode sizes and long propagation lengths suggests application to subwavelength devices such as visible nanolasers and terahertz lasers, as well as optically integrated circuits[19–22].

METHODS

COUPLED MODE THEORY

Coupled mode theory describes the mode hybridization of two uncoupled modes using a two-dimensional matrix representation. A linear superposition of basis vectors, which here represent the uncoupled SPP (without cylinder) and one of the degenerate cylinder (without metallic region) waveguide fundamental modes, defines two possible hybrid modes: $\psi_{\pm}(d,h) = a_{\pm}(d,h)\psi_{cyl}(d) + b_{\pm}(d,h)\psi_{spp}$, where $a_{\pm}(d,h)$ and $b_{\pm}(d,h)$ are the amplitudes of the constituent cylinder $\psi_{cyl}(d) = \{1 \quad 0\}^T$ and SPP $\psi_{spp} = \{0 \quad 1\}^T$ basis modes, respectively. All modes may be characterized in terms of an effective index, which is proportional to the real part of its eigenvalue quantifying the phase velocity in the direction of propagation $\hat{z}$ (Fig. 1). The magnitude of the in-plane surface plasmon wavevector, $k_{spp} = n_{spp}k_0$ corresponds to an effective index $n_{spp} = \sqrt{\varepsilon_m\varepsilon_d/(\varepsilon_m + \varepsilon_d)}$ (black dashed line in Fig. 4a)[2], where k_0 is the free-space wavenumber. The effective index of the fundamental cylinder mode, $n_{cyl}(d)$, is calculated using standard analytical means[29] (solid black line in Fig. 4a). The modes of the coupled system are characterized by the system of equations

$$\begin{pmatrix} n_{cyl}(d) & V(h,d) \\ V(h,d) & n_{spp} \end{pmatrix} \begin{pmatrix} a_{\pm}(d,h) \\ \sqrt{1-|a_{\pm}(d,h)|^2} \end{pmatrix} = n_{\pm}(d,h) \begin{pmatrix} a_{\pm}(d,h) \\ \sqrt{1-|a_{\pm}(d,h)|^2} \end{pmatrix}, \quad (3)$$

where $V(d,h)$ is the coupling strength between cylinder and SPP modes and mode amplitude normalization implies $b_{\pm}(d,h) = \sqrt{1-|a_{\pm}(d,h)|^2}$. The mode labels reflect the quadratic nature of the characteristic equation of the coupled mode theory, for which the solutions are $n_{\pm} = \bar{n}(d) \pm \Delta(d,h)$, where $\bar{n} = (n_{cyl}(d) + n_{spp})/2$ and $\Delta(d,h)^2 = (n_{cyl} - n_{spp})^2/4 + V(d,h)^2$. The mode amplitude $|a_+(d,h)|^2$ provides a measure of the character of the hybrid mode (Fig. 4b), that is, the degree to which the guided mode is cylinder-like (or for $1 - |a_+(d,h)|^2$, SPP-like), and is given by

$$|a_+(d,h)|^2 = \frac{V(d,h)^2}{(n_+(d,h) - n_{cyl}(d))^2 + V(d,h)^2}. \quad (4)$$

Equation (4) can be rewritten in the form presented in the main text (see equation (2)) using the solution for $n_+(d,h)$ and then equating $n_{hyb}(d,h) = n_+(d,h)$.

DEFINITION OF MODE AREA A_m AND PROPAGATION LENGTH L_m

The modal area A_m is defined as the ratio of the total mode energy and the peak energy density, such that

$$A_m = \frac{W_m}{\max\{W(\mathbf{r})\}} = \frac{1}{\max\{W(\mathbf{r})\}} \iint_{-\infty}^{\infty} W(\mathbf{r})\, d^2\mathbf{r}, \quad (5)$$

where W_m and $W(\mathbf{r})$ are the electromagnetic energy and energy density respectively (per unit length along the direction of propagation):

$$W(\mathbf{r}) = \frac{1}{2}\left(\frac{d(\varepsilon(\mathbf{r})\omega)}{d\omega}|E(\mathbf{r})|^2 + \mu_0|H(\mathbf{r})|^2\right) \quad (6)$$

Although this provides a fair measure of the confinement, the proportion of a mode's energy that propagates within A_m ultimately depends on the field distribution. Generally this is not arbitrarily quantifiable. In the current system, for $d = 200$ nm we have estimated this proportion to be more than 25% for $h = 2$ nm (Fig. 2e), and up to more than 60% for $h = 100$ nm (Fig. 2d). When interpreting these results, it is useful to note that the value of A_m is also the area of a uniform field distribution carrying the same energy density as the optical mode in question.

In the text, the normalized energy density $W(\mathbf{r})A_0/W_m$ is plotted in Fig. 4. This neatly emphasizes the reciprocal relationship of the peak normalized energy density and the normalized mode area A_m/A_0.

The propagation length is $L_m = 1/(2\,\mathrm{Im}\{k_{hyb}(d,h)\})$, where $k_{hyb}(d,h)$ is the complex-mode wavevector component in the propagation direction.

NUMERICAL CALCULATIONS

The hybrid mode's complex effective index $n_+(d,h)$ was calculated using the commercial finite-element package FEMLab from COMSOL. The eigenvalue solver was used to find modes of the hybrid waveguide. The effective index and

propagation distance were determined from the real and imaginary parts of the eigenvalue. The extremities of the calculation region were given scattering properties to mimic the necessary open boundary conditions. A convergence analysis was conducted to ensure that the real and imaginary parts of the effective indices varied by less than 1%. This corresponded to a calculation region between 4λ and 12λ in the $\hat{x}$-direction and 4λ in the $\hat{y}$-direction, depending upon the diameter d and gap width h ($\lambda = 1{,}550$ nm is the free-space wavelength.) Convergence of the numerical solution, for asymptotic values of d and h, with analytical solutions (compare with Fig. 5) indicates that the meshing, boundary conditions and associated calculation parameters were sound. Rapid convergence was achieved by using the uncoupled cylinder (that is, without the metallic region) effective index as an initial guess for large d, followed by successive refinement of the resulting solution for decreasing values of d for each value of h considered.

Received 17 March 2008; accepted 3 June 2008; published 11 July 2008.

References

1. Kirchain, R. & Kimerling, L. A roadmap for nanophotonics. *Nature Photonics* **1,** 303–304 (2007).
2. Boardman, A. D. *Electromagnetic Surface Modes* (Wiley, New York, 1982).
3. Barnes, W. L. Dereux, A. & Ebbesen, T. W. Surface plasmon subwavelength optics. *Nature* **424,** 824–830 (2003).
4. Takahara, J., Yamagishi, S., Taki, H., Morimoto, A. & Kobayashi, T. Guiding of a one-dimensional optical beam with nanometer diameter. *Opt. Lett.* **22,** 475–477 (1997).
5. Novotny, L. & Hafner, C. Light propagation in a cylindrical waveguide with a complex, metallic, dielectric function. *Phys. Rev. E.* **50,** 4094–4106 (1994).
6. Takahara, J. & Kobayashi, T. Nano-optical waveguides breaking through diffraction limit of light, in *Optomechatronic Micro/Nano Components, Devices, and Systems*, *Proc. SPIE*, vol. 5604, 158–172 (ed. Katagiri, Y.) (SPIE, Bellingham, WA, 2004).
7. Pile, D. F. P. & Gramotnev, D. K. Channel plasmon-polariton in a triangular groove on a metal surface. *Opt. Lett.* **29,** 1069–1071 (2004).
8. Govyadinov, A. A. & Podolskiy, V. A. Gain-assisted slow to superluminal group velocity manipulation in nanowaveguides. *Phys. Rev. Lett.* **97,** 223902 (2006).
9. Silveirinha, M. & Engheta, N. Tunneling of electromagnetic energy through subwavelength channels and bends using ε-near-zero materials. *Phys. Rev. Lett.* **97,** 157403 (2006).
10. Maier, S. A. *et al.* Local detection of electromagnetic energy transport below the diffraction limit in metal nanoparticle plasmon waveguides. *Nature Mater.* **2,** 229–232 (2003).
11. Bozhevolnyi, S. I., Volkov, V. S., Devaux, E. & Ebbesen, T. W. Channel plasmon-polariton guiding by subwavelength metal grooves. *Phys. Rev. Lett.* **95,** 046802 (2005).
12. Pile, D. F. P. *et al.* Two-dimensionally localized modes of a nanoscale gap plasmon waveguide. *Appl. Phys. Lett.* **87,** 261114 (2005).
13. Steinberger, B. *et al.* Dielectric stripes on gold as surface plasmon waveguides. *Appl. Phys. Lett.* **88,** 094104 (2006).
14. Cregan, R. F. *et al.* Single-mode photonic band gap guidance of light in air. *Science* **285,** 1537–1539 (1999).
15. Wiederhecker, G. S. *et al.* Field enhancement within an optical fibre with a subwavelength air core. *Nature Photonics* **1,** 115–118 (2007).
16. Altug, H., Englund, D. & Vuckovic, J. Ultrafast photonic crystal nanocavity laser. *Nature Phys.* **2,** 484–488 (2006).
17. Almeida, V. R., Xu, Q., Barios, C. A. & Lipson, M. Guiding and confining light in void nanostructure. *Opt. Lett.* **29,** 1209–1211 (2004).
18. Genov, D. A., Ambati, M. & Zhang, X. Surface plasmon polariton amplification in planar metal films. *IEEE J. Quant. Electron.* **43,** 1104–1108 (2007).
19. Huang, M. H. *et al.* Room-temperature ultraviolet nanowire nanolasers. *Science* **292,** 1897–1899 (2001).
20. Hill, M. T. *et al.* Lasing in metallic-coated nanocavities. *Nature Photonics* **1,** 589–594 (2007).
21. Williams, B. S. Terahertz quantum cascade lasers. *Nature Photonics* **1,** 517–525 (2007).
22. Almeida, V. R., Barrios, C. A., Panepucci, R. R. & Lipson, M. All-optical control of light on a silicon chip. *Nature* **431,** 1081–1084 (2004).
23. Huang, Y. & Lieber, C. Integrated nanoscale electronics and optoelectronics: Exploring nanoscale science and technology through semiconductor nanowires. *Pure Appl. Chem.* **76,** 2051–2068 (2004).
24. Johnson, P. B. & Christie, R. W. Optical constants of the noble metals. *Phys. Rev. B* **6,** 4370–4379 (1972).
25. Kou, F. Y. & Tamir, T. Range extension of surface plasmons by dielectric layers. *Opt. Lett.* **12,** 367–369 (1987).
26. Jackson, J. D. *Classical Electrodynamics* 3rd edn (John Wiley & Sons, New York, 1999).
27. Prodan, E., Radloff, C., Halas, N. J. & Nordlander, P. A Hybridization model for the plasmon response of complex nanostructures. *Science* **302,** 419–422 (2003).
28. Nordlander, P. & Le, F. Plasmonic structure and electromagnetic field enhancements in the metallic nanoparticle-film system. *J. Appl. Phys. B* **84,** 35–41 (2006).
29. Snyder, A. W. & Love, J. D. *Optical Waveguide Theory* (Chapman & Hall, London, New York, 1983).
30. Buckley, R. & Berini, P. Figures of merit for 2D surface plasmon waveguides and application to metal stripes. *Opt. Express* **15,** 12174–12182 (2007).

Supplementary Information accompanies this paper at www.nature.com/naturephotonics.

Acknowledgements

The authors thank G. Bartal for valuable discussions. This work was supported by the Air Force Office of Scientific Research (AFOSR), the Multidisciplinary University Research Initiative (MURI) (FA9550-04-1-0434) and the National Science Foundation (NSF) Nanoscale Science and Engineering Center (DMI-0327077).

Author contributions

R.F.O. conceived of the original concept and carried out the calculations. All authors contributed equally in developing the concept and writing the manuscript.

Author information

Reprints and permission information is available online at http://npg.nature.com/reprintsandpermissions/. Correspondence and requests for materials should be addressed to X.Z.